Solar Physics
DOI: 10.1007/•••••-•••-•••-••••-•

Horizontal Flows in the Photosphere and Subphotosphere of Two Active Regions

Yang Liu[1] · **Junwei Zhao**[1] · **P.W. Schuck**[2]

Abstract We compare horizontal flow fields in the photosphere and subphotosphere a layer of 0.5 Mm below the photosphere in two solar active regions: AR 11084 and AR 11158. AR 11084 is a mature, simple active region without significant flaring activities, and AR 11158 is a multipolar, complex active region with magnetic flux emerging during the period studied. Flows in the photosphere are derived by applying the method of Differential Affine Velocity Estimator for Vector Magnetograms (DAVE4VM) on HMI observed vector magnetic fields, and the subphotospheric flows are inferred by time – distance helioseismology using HMI observed Doppergrams. Similar flow patterns are found for both layers for AR 11084: inward flows in sunspot umbra and outward flows surrounding the sunspot. The boundary between the inward and outward flows, which is slightly different in the photosphere and the subphotosphere, is within the sunspot penumbra. The area having inward flows in the subphotosphere is larger than that in the photosphere. For AR 11158, flows in these two layers show great similarities in some areas and significant differences in other areas. Both layers exhibit consistent outward flows in the areas surrounding sunspots. On the other hand, most well-documented flux-emergence-related flow features seen in the photosphere do not have their counterparts in the subphotosphere. This implies that the horizontal flows caused by flux emergence do not extend deeply into the subsurface.

Keywords: Solar active regions, photosphere and subphotosphere; Solar active regions, flows

1. Introduction

Plasma flows in the solar photosphere are of great importance to understand the dynamics in the solar photosphere and to study connections of photospheric flow fields and solar flaring activities. Different methods have been developed to derive

[1] W. W. Hansen Experimental Physics Laboratory, Stanford University, Stanford, CA 94305-4085, USA email: yliu@sun.stanford.edu
[2] Solar Physics Laboratory, NASA Goddard Space Flight Center, Greenbelt, MD 20771, USA

flow fields in the photosphere. Local correlation tracking, initially developed by November and Simon (1988), has been widely used to study velocities inside supergranules and active regions. Different types of feature tracking methods (*e.g.*, Hagenaar *et al.*, 1999) were also developed to study various aspects of the solar dynamics, including magnetic-flux fragmentation and merging, determination of statistical parameters of solar dynamos, and others. Comparisons among different feature-tracking methods were also carried out (DeForest *et al.*, 2007), and it was found that the results from these different methods were in reasonable agreement. It was also realized by many authors that the magnetic feature-tracking method might not be valid when there were magnetic-flux emergence or other complicated activities occurring inside the studied active regions. Therefore some new methods, with the magnetic-induction equation taken into account, were developed to enhance the reliability of the inferred flow fields in such regions (Kusano *et al.*, 2002; Longcope, 2004; Welsch *et al.*, 2004; Georgoulis and LaBonte, 2006; Schuck, 2008).

Meanwhile, with the rapid development of helioseismology, mapping subsurface plasma flows has become possible for ring-diagram analysis (*e.g.*, Komm *et al.*, 2005) and for time – distance helioseismology (*e.g.*, Zhao *et al.*, 2012). In particular, time – distance helioseismology provides a high spatial-resolution inference of subsurface flow field, which has allowed studies of supergranules and active regions. In fact, the subsurface flow fields obtained from time – distance measurements have also been compared with the results derived from local correlation tracking for the quiet Sun (De Rosa, Duvall, and Toomre, 2000; Švanda, Zhao, and Kosovichev, 2007), and reasonable agreements were reported. However, a systematic comparison of photospheric and subphotospheric flows derived for active regions has not yet been carried out.

In this article, we carry out a comparison between photospheric flows and subphotospheric flows inside two selected active regions, and try to understand the similarities and discrepancies of these results. The photospheric flow field is obtained from Differential Affine Velocity Estimator for Vector Magnetograms (DAVE4VM; Schuck 2008) using the data of HMI observed vector magnetograms. The subphotospheric flow field is from HMI time – distance analysis pipeline (Zhao *et al.*, 2012) using the HMI Doppler velocity, but only results from the shallowest depth, i.e. a depth range of $0 - 1$ Mm (hereafter, -0.5 Mm for a simpler description), are used. It is very interesting to see how the results from these two very different analysis techniques using different data inputs agree or differ. Moreover, the differences in the flow fields between different depths shed some light in understanding the rapidly developing complex active regions and flaring activities inside these regions. We introduce the procedure of data reductions in Section 2, and present our results in Section 3, together with a brief discussion. Conclusions are given in Section 4.

2. Data Reduction

We use Doppler velocity and vector magnetic field data taken by HMI (Scherrer *et al.*, 2012; Schou *et al.*, 2012) to derive subsurface flow field and photospheric flow field,

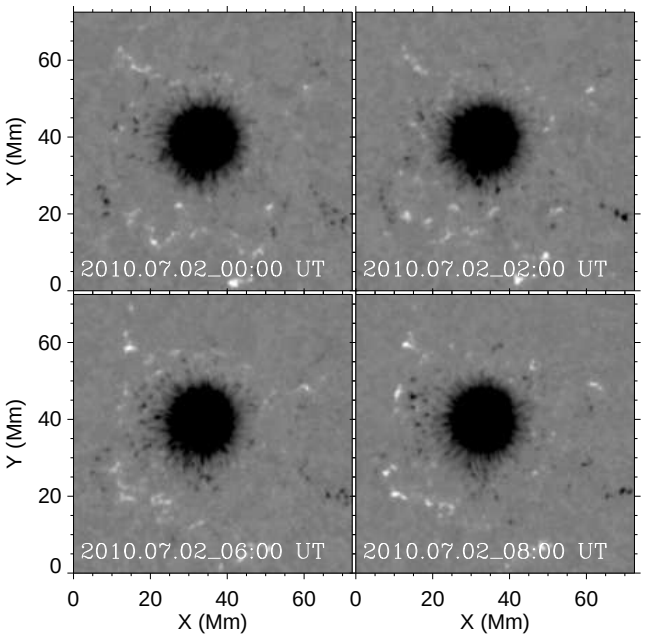

Figure 1. Vertical magnetic field in active region AR 11084 at 00:00 UT, 02:00 UT, 06:00 UT, and 08:00 UT of 2 July 2010. Black and white refer to negative and positive fields, respectively.

respectively. The HMI instrument is a filtergraph with a full-disk coverage of 4096×4096 pixels. The spatial resolution is about 1″ with a 0.5″ pixel size. The spectral line is Fe I 6173 Å absorption line formed in the photosphere (Norton *et al.*, 2006). There are two CCD cameras in the instrument, the "front camera" and the "side camera". The front camera acquires the filtergrams at six wavelengths along the line Fe I 6173 Å in two polarization states with 3.75 seconds between the images. It takes 45 seconds to acquire a set of 12 filtergrams. This set of data is used to derive Dopplergrams and line-of-sight magnetograms (Couvidat *et al.*, 2012). The side camera is dedicated to measuring the vector magnetic field. It takes 135 seconds to obtain the filtergrams in six polarization states at six wavelength positions. The Stokes parameters [*I, Q, U, V*] are then computed from those measurements. In order to suppress the *p*-mode oscillations and increase the signal-to-noise ratio, the Stokes parameters are usually derived from the filtergrams averaged over a certain period of time. Currently an average is computed every 720 seconds. This average needs extra filtergrams before and after the nominal 720-second temporal window because the filtergrams need to be interpolated onto a regular and finer grid before averaging. The averaging uses a cosine-apodized boxcar with a Full Width Half Maximum (FWHM) of 720-second. The tapered temporal window used is actually 1215 seconds. The Stokes parameters are then inverted to produce the vector magnetic field using the

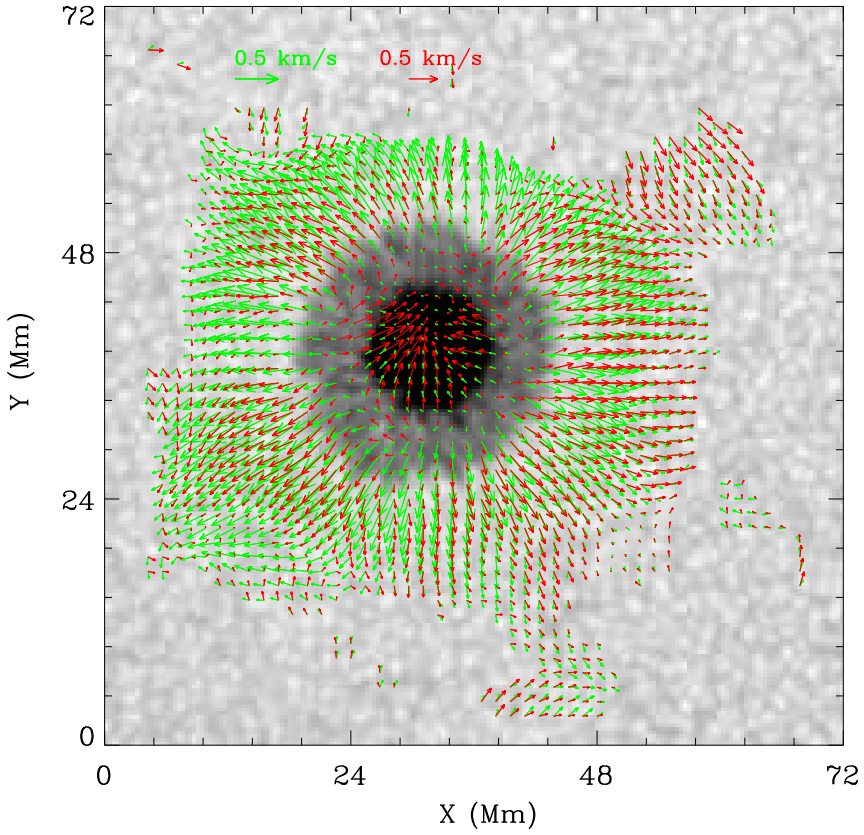

Figure 2. Horizontal flows in AR 11084 in the photosphere (green arrows) and in the −0.5 Mm layer (red arrows) overplotted on a continuum-intensity image taken at 2 July 2010 02 04:00 UT. The photospheric flow is an average of eight velocity maps at a cadence of one-hour from 00:00 UT to 08:00 UT derived by DAVE4VM. The flow in the −0.5 Mm layer is derived by a time – distance helioseismology method applied to eight-hour Dopplergrams observed from 2 July 2010 00:00 UT to 08:00 UT. Only velocities at locations where the horizontal velocity in the photosphere is greater than 0.07 km s^{-1} are plotted.

Very Fast Inversion of the Stokes Vector (VFISV) inversion algorithm, a Milne-Eddington (ME) based approach (Borrero *et al.*, 2011). The 180° ambiguity of the azimuth is solved based on the "minimum energy" algorithm (Metcalf, 1994; Metcalf *et al.*, 2006; Leka *et al.*, 2009). The disambiguated vector magnetic-field data of active regions are finally deprojected into the heliographic coordinates.

DAVE4VM (Schuck, 2008) is used to derive the vector velocity field in the photosphere from HMI time-series deprojected, registered vector magnetic-field data. The cadence of the data is 720 seconds. The window size used in DAVE4VM is 19 pixels, which is determined by examining slope, Pearson linear correlation coefficient, and Spearman rank order between $\bigtriangledown_h \cdot (v_z \mathbf{B}_h - \mathbf{v}_h B_z)$ and $\delta B_z / \delta t$,

where v_z and $\mathbf{v}_h$ are vertical and horizontal velocities, and B_z and $\mathbf{B}_h$ are vertical and horizontal magnetic fields, as suggested in Schuck (2008).

The subphotospheric flow fields are obtained from HMI time – distance data-analysis pipeline, and all analysis details of the technique and an example of subphotospheric flow field of one active region can be found in Zhao *et al.* (2012). The data input for such a pipeline analysis is HMI observed Dopplergrams with a sampling rate of 0.12° pixel^{-1}. Although the pipeline provides subsurface flow fields down to 20 Mm in depth, here we only use the shallowest depth, *i.e.* -0.5 Mm for a direct comparison with the photospheric flow fields.

We select two active regions to carry out this comparison. One is a mature yet simple active region, AR 11084; the other is an emerging, multipolar, and complicated active region, AR 11158. The time – distance helioseismology method needs eight-hour Doppler velocities to derive the horizontal velocity field in the subsurface. Thus it is deemed to be an average velocity during that eight-hour time interval. For AR 11084, we use data during the period of 2 July 2010 00:00 UT to 08:00 UT, and for AR 11158, the data used cover from 14 February 2011 06:00 UT to 14:00 UT. For the velocity in the photosphere, DAVE4VM can provide the velocity field at a cadence of 720 seconds, the same as that for HMI vector magnetic field data. For the purpose of comparison, we average eight derived photospheric velocity fields during that eight-hour time interval, one per hour, to obtain an eight-hour averaged photospheric velocity field. This velocity field is used to compare with the velocity obtained for the -0.5 Mm layer.

3. Results and Discussions

3.1. AR 11084

AR 11084 is a mature simple active region with a stable and relatively round sunspot located inside it. Figure 1 shows the evolution of magnetic field in AR 11084 in the eight hours during which the study is carried out, and no significant evolution is seen during this eight-hour interval for the sunspot.

Figure 2 shows horizontal flows in this active region plotted on a continuum intensity image. The arrows represent the flows in the photosphere (green) and in the -0.5 Mm layer (red), respectively. Only velocities where the horizontal speed in the photosphere is greater than 0.07 km s^{-1} are plotted. Please note that the scales are slightly different in two maps in order to better display the results. In general, both maps show very similar flow patterns: inward-flows in the sunspot umbra and outward flows in the areas surrounding the sunspot. The inward- and outward-flows pattern in mature sunspots in the photosphere was previously reported in, *e.g.*, Schröter (1962), Muller (1973), and Wang and Zirin (1992). Separation of the inward- and outward-flows takes place in the sunspot penumbra. But the boundaries between the two opposite-flow directions are different in these two layers. The area having inward flows at the -0.5 Mm layer is larger than that in the photosphere. In other words, the flows in the penumbra that have already become outflows in the photosphere are still inward-flow at the -0.5 Mm layer. This inward-flow may play a role in containing the sunspot (Zhao *et al.*, 2010).

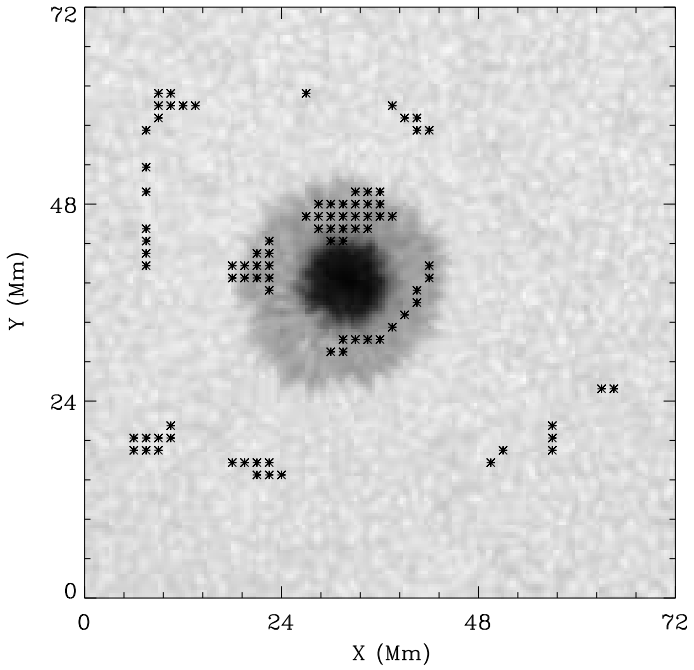

Figure 3. Background image is the 2 July 2010 04:00 UT continuum intensity data. Asterisks refer to the areas where the angle between the two flows in the photosphere and the −0.5 Mm layer is greater than 90°.

To better illustrate difference of the flows in these two layers, we mark with asterisks in Figure 3 the locations where the angle between the two flows is greater than 90°. It shows that the major differences between these two sets of results are inside the sunspot penumbra and other areas far away from the sunspot, where the method DAVE4VM becomes insensitive due to weak magnetic field strength.

While there are a few areas that show different flows in the two layers, the majority of the areas actually shows very similar flow patterns in both layers. Figure 4 shows scatter plots of the velocities in the two layers. In the top panels are scatter plots of v_x (right) and v_y (left). Magnitude ($|v| = \sqrt{v_x^2 + v_y^2}$) and azimuthal angle [$\theta$] of horizontal velocity are plotted in the bottom panels. The azimuthal angle ranges from −180° to 180°. The horizontal axis represents velocity in the −0.5 Mm layer from the time – distance helioseismology technique, and the vertical axis in the photosphere from the DAVE4VM method. The Pearson correlation coefficient is 0.89 for v_x, 0.76 for v_y, 0.48 for $|v|$, and 0.64 for θ. The v_x has a better correlation than v_y, and this was also reported by Švanda, Zhao, and Kosovichev (2007) for the quiet-Sun study. Poor correlation in $|v|$ implies a gradient between the two layers. We also calculate the vector correlation coefficient and Cauchy – Schwarz inequality (Schrijver *et al.*, 2006).

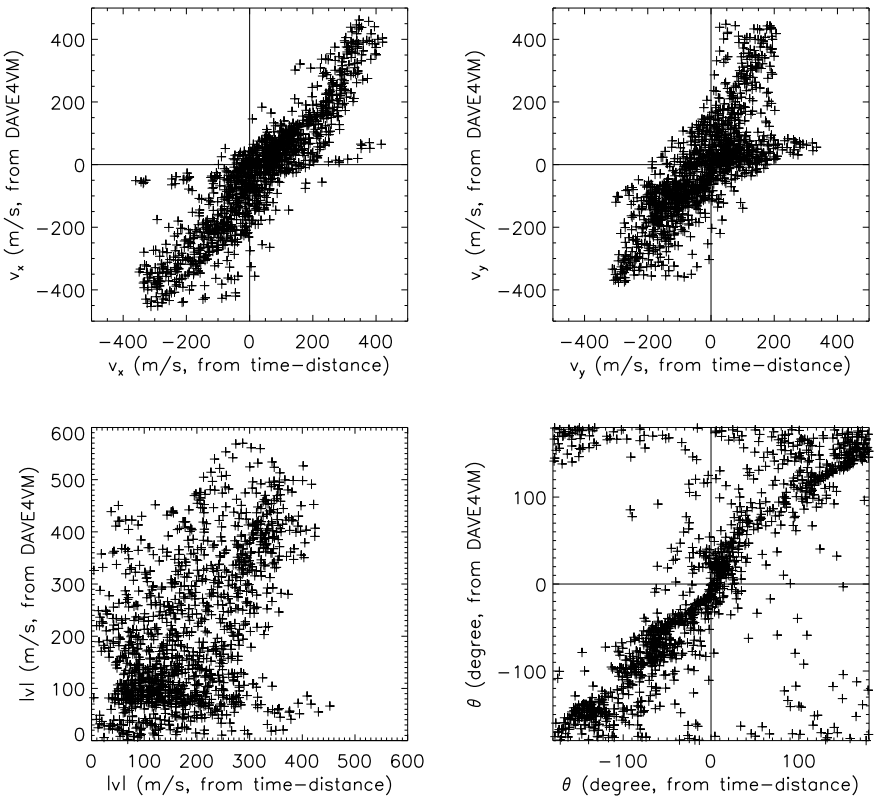

Figure 4. Scatter plots between the velocities of two layers for v_x (top left), v_y (top right), their magnitudes ($|v|$; bottom left) and azimuthal angles (θ; bottom right). Horizontal axis represents velocity in the -0.5 Mm layer from the time – distance helioseismology method, while the vertical axis in the photosphere from the DAVE4VM. The Pearson correlation coefficient is 0.89 for v_x, 0.76 for v_y, 0.48 for $|v|$, and 0.64 for θ, respectively.

Vector correlation coefficient C_{vec} is defined as

$$C_{vec} = \frac{\sum_i \mathbf{v}_i \cdot \mathbf{u}_i}{(\sum_i \mathbf{v}_i{}^2 \sum_i \mathbf{u}_i{}^2)^{1/2}}, \tag{1}$$

where $\mathbf{v}_i$ and $\mathbf{u}_i$ are velocities in two layers at pixel i. The Cauchy – Schwarz inequality C_{cs} is defined as

$$C_{cs} = \frac{1}{M} \sum_i \frac{\mathbf{v}_i \cdot \mathbf{u}_i}{|\mathbf{v}_i||\mathbf{u}_i|}, \tag{2}$$

where M is the total number of pixels in the region studied. Here we use only two components of vector velocity field, *i.e.*, the horizontal velocity, to compute the coefficients. The vector correlation coefficient is 0.80 and the Cauchy-Schwarz inequality is 0.76. This indicates that the flows in the two layers are very similar.

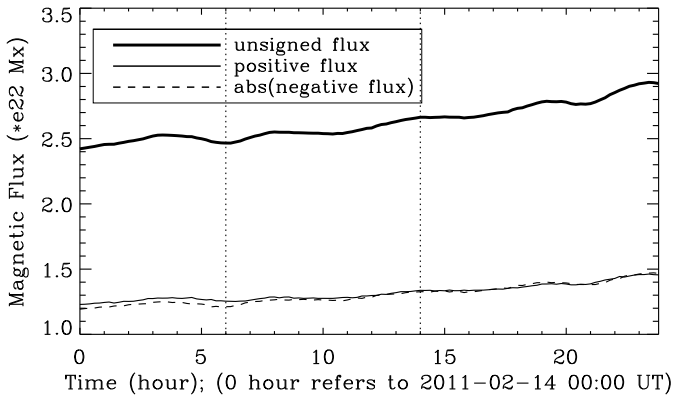

Figure 5. Temporal profiles of magnetic flux in AR 11158 on 14 February 2011. Thick solid line represents unsigned flux, while solid and dashed lines are positive flux and absolute value of negative flux. Vertical magnetic fields greater than 100 Gauss, the noise level of magnetic field strength, are used to measure the fluxes. Two vertical dotted lines mark the time interval from 06:00 UT to 14:00 UT in which the flows are analyzed here.

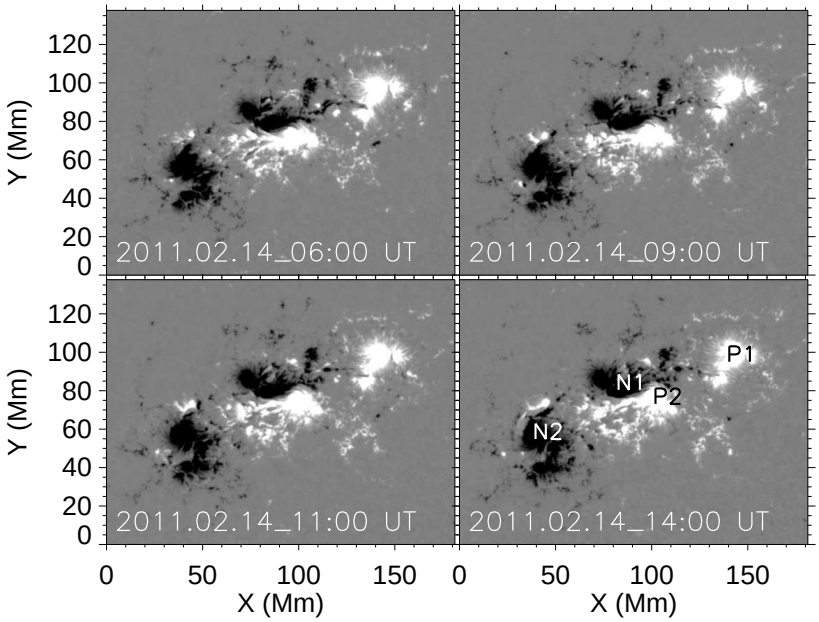

Figure 6. Evolution of magnetic field in AR 11158 during 06:00 UT – 14:00 UT 14 February 2011. White and black represent positive and negative vertical magnetic fields, respectively. *P1* and *P2* in the bottom-right panel denotes positive polarity patches, while *N1* and *N2* negative field patches.

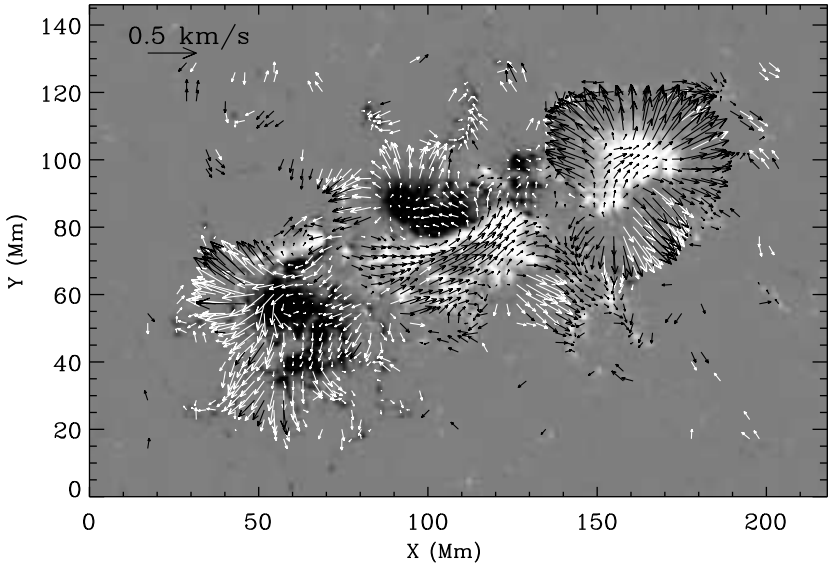

Figure 7. Horizontal velocity in the photosphere in AR 11158 derived by DAVE4VM. The image is vertical magnetic field with positive field in white and negative field in black. The arrows represent horizontal velocity. It is an average of eight velocity maps at a cadence of one-hour from 06:00 UT – 14:00 UT 14 February 2011. Only velocity greater than 0.07 km s^{-1} is plotted. Black (white) arrows indicate that the vertical magnetic fields in the pixels are positive (negative).

3.2. AR 11158

AR 11158 is a multipolar, complex active region, producing several major flares during its disk passage (*e.g.*, Sun *et al.* 2012). The flows studied here in the photosphere are an average of eight one-hour cadence flow maps derived by DAVE4VM for the period of 14 February 2011 06:00 UT to 14:00 UT, during which magnetic flux was emerging in this region. This is demonstrated by the temporal profiles of magnetic-flux evolution in the region (see Figure 5). The two vertical dotted lines mark the time interval during which the flows are calculated. It is also seen that the positive and negative fluxes are well balanced. Shown in Figure 6 is the vertical magnetic field in AR 11158 in this eight-hour time interval. The negative field patches *N1* and *N2* (see the bottom-right panel) rotate counter-clockwise, while the positive field patch *P1* (leading polarity) undergoes separation, moving towards the Northwest. Shear motion along the polarity inversion line between *N1* and *P2* is also clearly seen. These flow patterns are confirmed by the photospheric flow map by DAVE4VM (see Figure 7).

Flows in AR 11158 in the photosphere and at the −0.5 Mm layer are compared in Figure 8. Outward flows are clearly seen in the areas surrounding the sunspots in both layers, as also seen in AR 11084. However, the well-documented flux-emergence-related surface flows in the photosphere (*e.g.* Brown *et al.*, 2003, Zhang *et al.*, 2007, Schmieder *et al.*, 1994, Deng *et al.*, 2006) – the rotation of

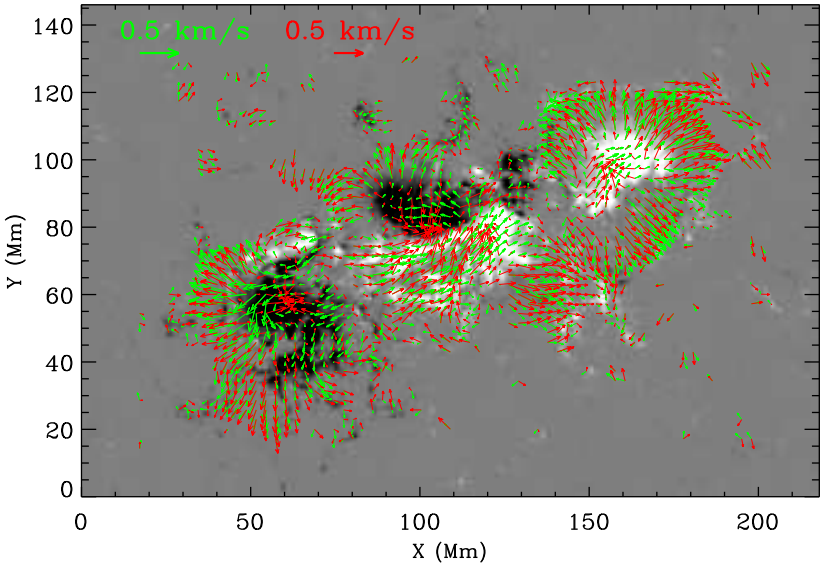

Figure 8. Vertical magnetic field in AR 11158 (image) overplotted by the horizontal velocities in the photosphere (green arrows) and in the −0.5 Mm layer (red arrows). Black and white in the image refer to negative and positive fields, respectively. The photospheric velocity is the same as in Figure 7. The flow in the −0.5 Mm layer is derived by a time – distance helioseismology method applied to eight-hour Dopplergrams observed from 06:00 UT – 14:00 UT 14 February 2011. Only velocities at locations where the horizontal velocity in the photosphere is greater than 0.07 km s^{-1} are plotted.

negative field patches *N1* and *N2*, the separation motion of positive field patch *P1*, and the shear motion along the polarity inversion line between *P2* and *N1*– do not have their counterparts in the −0.5 Mm layer. Instead, significant inward-flows in the sunspots are seen (*e.g.* in *N1*, *N2* and *P1*). Figure 9 shows the flow fields in these patches in detail. Figure 10 is another way to show the difference of flows in the two layers: the asterisks mark areas where the angle between the two flows is greater than 90°. Significant difference occurs in the rotational sunspots, *N1* and *N2*, and in the separation-motion sunspot *P1*. This indicates that the surface flows in the photosphere that are related to flux emergence do not extend very deeply into the subsurface. Those flows are probably caused by the magnetic field, which is emerging and expanding into the solar corona. Gradients in magnetic field due to its rapid emergence and expansion drive motions in the photosphere, as demonstrated in MHD simulations (*e.g.* Magara and Longcope, 2003, Manchester *et al.*, 2004, Fan, 2009). This has less effect in the subphotosphere.

The scatter plots of velocities in two layers in AR 11158 are presented in Figure 11. As expected, the correlation coefficient is lower than that for AR 11084. Once again, the v_x has a better correlation than v_y.

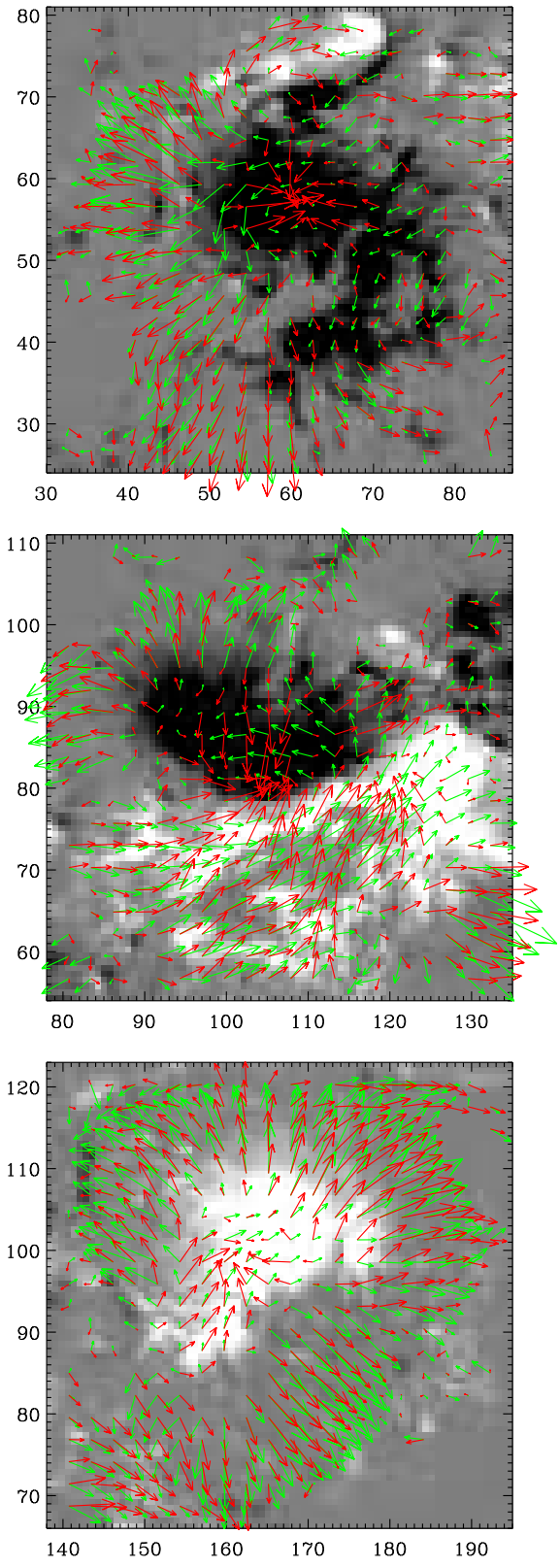

Figure 9. Enlarged sub-areas of Figure 8 to show details in the three interesting regions that include patch *N2* (top), patches *N1* and *P2*, (middle), and patch *P1* (bottom) marked in Figure 6. Both vertical and horizontal axises are in Mm.

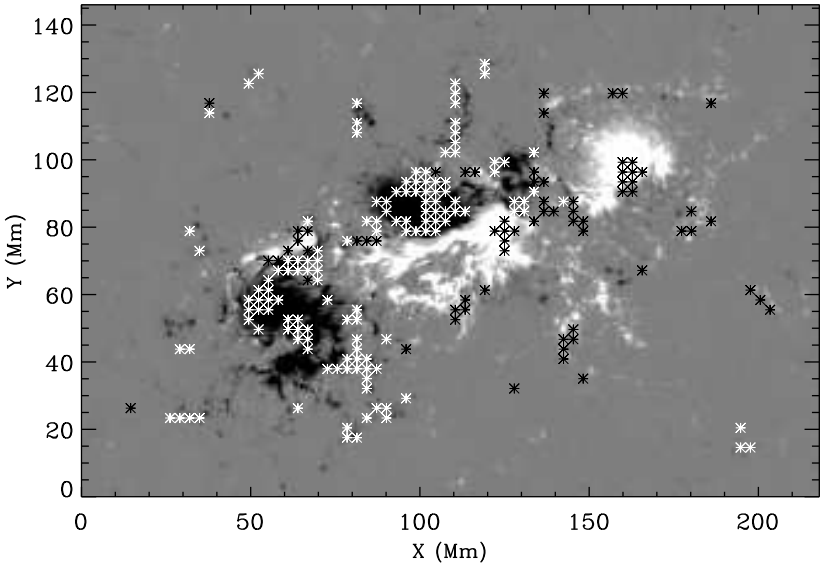

Figure 10. Background image is the vertical magnetic field in AR 11158. Asterisks represent the areas where the angle between the horizontal velocities in the photosphere and the −0.5 Mm layer is greater than 90°. White (black) asterisk refers to the area where the vertical field is negative (positive).

3.3. Discussions

For both active regions, we also extend the subsurface flows, obtained from the time – distance data-analysis pipeline, down to −6 Mm in depth to compare with the −0.5 Mm flow fields. For the depth down to −3 Mm, the flow patterns look quite similar to that −0.5 Mm, indicating that similar flow structures extend to a depth of −3 Mm or so. Below −3 Mm, the outflow structure beyond the sunspot penumbra remains largely unchanged, but the inflow structure inside the penumbra has changed to outflows. The depth variation of subsurface flow fields obtained from time – distance analysis has been discussed by various authors (*e.g.*, Zhao *et al.*, 2010). This large-scale outflows in sunspots have been reproduced by MHD numerical simulations. For example, Rempel (2011) showed that the large-scale outflows, extending from the photosphere to the deep interior, were associated with the sunspot penumbra. His simulation also showed converging flows in a sunspot without a penumbra. For a sunspot with a well-developed penumbra, however, no obvious converging flows were found in that simulation, which is not consistent with what we have shown here that the converging flows are in the umbra and part of the penumbra for both layers. This discrepancy deserves more study.

We also compared the vertical flows derived from both techniques, but found poor correlation between the two. The photospheric vertical flows in sunspots derived from DAVE4VM are dominated by upward flows, consistent with the strong outflows in the penumbra known as the Evershed effect. However, the

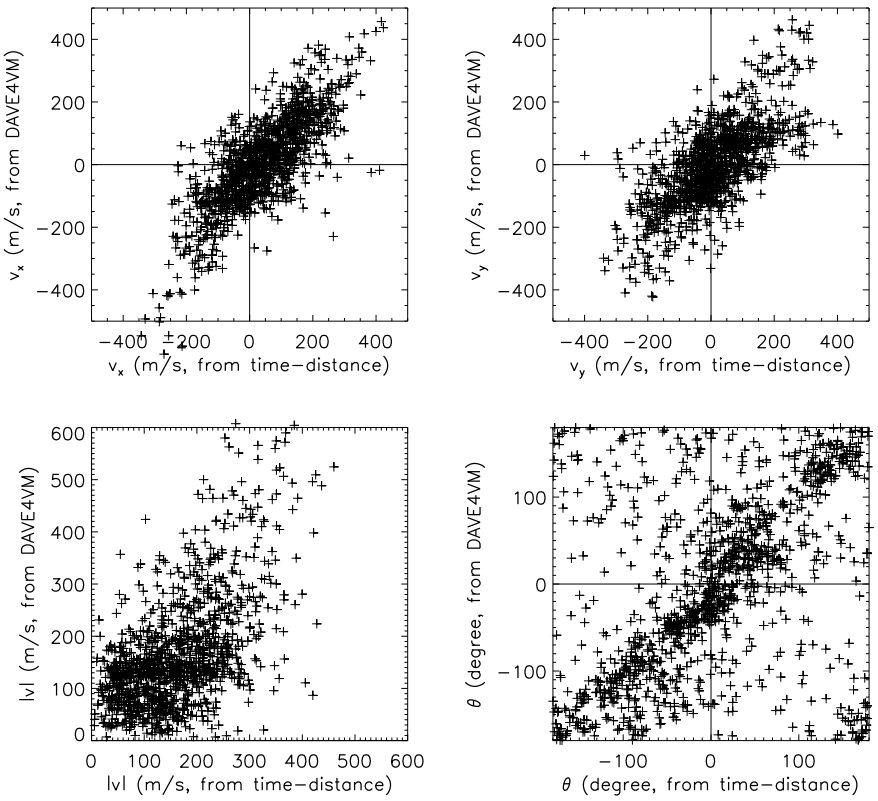

Figure 11. Scatter plots between the velocities of two layers for v_x (top left), v_y (top right), their magnitudes ($|v|$; bottom left) and azimuthal angles (θ; bottom right), for AR 11158. Horizontal axis represents velocity in the -0.5 Mm layer from the time – distance helioseismology method, while the vertical axis in the photosphere from the DAVE4VM. The Pearson correlation coefficient is 0.78 for v_x, 0.70 for v_y, 0.56 for $|v|$, and 0.43 for θ, respectively. Vector correlation coefficient for two components (horizontal velocity) is 0.73, and Cauchy – Schwarz inequality is 0.59.

subsurface vertical flows derived from time – distance analysis are dominated by downward flows, as discussed by Hindman, Haber, and Toomre (2009) and Zhao *et al.* (2010).

4. Conclusions

We compare flows in the photosphere and in the -0.5 Mm layer in two active regions. One is a mature simple active region and the other is an emerging, complex active region. We found that for the mature simple active region the flows in both layers show very similar patterns: inward-flow in the sunspot umbra and outward-flow in the areas surrounding the sunspot. The boundary separating these two types of flows occurs in the sunspot penumbra, but the

location of separation is slightly different in the two layers. The inward-flow area in the sunspot is larger in the −0.5 Mm layer than that in the photosphere. In other words, the flows in these areas where there are inward-flows in the −0.5 Mm layer have become outward-flow in the photosphere. Inward-flow in the sunspots in the subsurface is suggested to play a role in containing the sunspots (Zhao *et al.*, 2010).

For the emerging, complex active region, the flows in the two layers show both great similarity and significant difference. Though both layers show similar outward flows in the areas surrounding the sunspots, the well-documented flux-emergence-related surface flows seen in the photosphere, such as separation motion of leading and following polarity patches, fast rotation of sunspots, and apparent shear motion along the polarity inversion lines, do not have their counterparts in the −0.5 Mm layer. This implies that the cause for these flows, which is probably the gradient of magnetic field due to its rapid emergence and expansion into the corona, has less effect in the subsurface.

Acknowledgements The authors wish to thank the anonymous referee for the valuable comments and suggestions. This work was supported by NASA Contract NAS5-02139 (HMI) to Stanford University. The data have been used by courtesy of NASA/SDO and the HMI science team. SOHO is a project of international cooperation between ESA and NASA.

References

Borrero, J.M., Tomczyk, S., Kubo, M., Socas-Navarro, H., Schou, J., Couvidat, S., Bogart, R.: 2011, *Solar Phys.* ADS: 2011SoPh..273..267B, DOI: 10.1007/s11207-010-9515-6. **273**, 267.

Brown, D.S., Nightingale, R.W., Alexander, D., Schrijver, C.J., Metcalf, T.R., Shine, R.A., Title, A.M., Wolfson, C.J.: 2003, *Solar Phys.* **216**, 79. ADS: 2003SoPh..216...79B, DOI: 10.1023/A:1026138413791.

Couvidat, S. Rajaguru, S.P., Wachter, R., Sankarasubramanian, K., Schou, J. Scherrer, P.H.: 2012, *Solar Phys.* **278**, 217.

DeForest, C.E., Hagenaar, H.J., Lamb, D.A., Parnell, C.E., Welsch, B.T.: 2007, *Astrophys. J.* **666**, 576

Deng, N., Xu, Y., Yang, G., Cao, W., Liu, C., Rimmele, T.R., Wang, H., Denker, C.: 2006, *Astrophys. J.* **644**, 1278.

De Rosa, M., Duvall, T.L., Jr, Toomre, J.: 2000, *Solar Phys.* **192**, 351. ADS: 2000SoPh..192..351R, DOI: 10.1023/A:1005269001739.

Fan, Y.: 2009, *Astrophys. J.* **697**, 1529.

Georgoulis, M.K., LaBonte, B.J.: 2006, *Astrophys. J.* **636**, 475.

Hagenaar, H.J., Schrijver, C.J., Title, A.M., Shine, R.A.: 1999, *Astrophys. J.* **511**, 932.

Hindman, B.W., Haber, D.A., Toomre, J.: 2009, *Astrophys. J.* **698**, 1749.

Komm, R., Howe, R., Hill, F., González Hernández, I., Toner, C., Corbard, T.: 2005, *Astrophys. J.* **631**, 636.

Kusano, K., Maeshiro, T., Yokoyama, T., Sakurai, T., 2002, *Astrophys. J.* **577**, 501.

Leka, K.D., Barnes, G., Crouch, A.D., Metcalf, T.R., Gary, G.A., Jing, J., Liu, Y.: 2009, *Solar Phys.* **260**, 83. ADS: 2009SoPh..260...83L, DOI: 10.1007/s11207-009-9440-8.

Longcope, D.W.: 2004, *Astrophys. J.* **612**, 1181.

Magara, T., Longcope, D.W.: 2003, *Astrophys. J.* **586**, 630.

Manchester, W., IV, Gombosi, T., DeZeeuw, D., Fan, Y.: 2004, *Astrophys. J.* **610**, 588.

Metcalf, T.R.: 1994, *Solar Phys.* **155**, 235. ADS: 1994SoPh..155..235M, DOI: 10.1007/BF00680593.

Metcalf, T.R., Leka, K.D., Barnes, G. Lites, B.W., Georgoulis, M.K., Pevtsov, A.A., Balasubramaniam, K.S., Gary, G.A., Jing, J., Li, J., Liu, Y., Wang, H.N., Abramenko, V., Yurchyshyn, V., Moon, Y.-J.: 2006, *Solar Phys.* **237**, 267. ADS: 2006SoPh..237..267M, DOI: 10.1007/s11207-006-0170-x.

Muller, R.: 1973, *Solar Phys.* **29**, 55. ADS: 1973SoPh...29...55M, DOI: 10.1007/BF00153440.
Norton, A.A., Graham, J.P., Ulrich, R.K., Schou, J., Tomczyk, S., Liu, Y., Lites, B.W., López Ariste, A., Bush, R.I., Socas-Navarro, H., Scherrer, P.H.: 2006, *Solar Phys.* **239**, 69. ADS: 2006SoPh..239...69N, DOI: 10.1007/s11207-006-0279-y.
November, L.J., Simon, G.W.: 1988, *Astrophys. J.* **333**, 427
Pesnell, P.D., Thompson, B.J., Chamberlin, P.C.: 2012, *Solar Phys.* **275**, 3. ADS: 2012SoPh..275....3P, DOI: 10.1007/s11207-011-9841-3.
Rempel, M.: 2011, *Astrophys. J.* **740**, 15.
Schuck, P.W.: 2008, *Astrophys. J.* **683**, 1134.
Scherrer, P.H., Bogart, R.S., Bush, R.I., Hoeksema, J.T., Kosovichev, A.G., Schou, J., Rosenberg, W., Springer, L., Tarbell, T.D., Title, A., Wolfson, C.J., Zayer, I., and MDI Engineering Team: 1995, *Solar Phys.* **162**, 129. ADS: 1995SoPh..162..129S, DOI: 10.1007/BF00733429.
Scherrer, P.H., Schou, J., Bush, R.I., Kosovichev, A.G., Bogart, R.S., Hoeksema, J.T., Liu, Y., Duvall, T.L. Jr, Zhao, J., Title, A.M., Schrijver, C.J., Tarbell, T.D., Tomczyk, S.: 2012, *Solar Phys.*, **275**, 207. ADS: 2012SoPh..275..207S, DOI: 10.1007/s11207-011-9834-2.
Schou, J., Scherrer, P.H., Bush, R.I., Wachter, R., Couvidat, S., Rabello-Soares, M.C., Bogart, R.S., Hoeksema, J.T., Liu, Y., Duvall, T.L. Jr., Akin, D.J., Allard, B.A., Miles, J.W., Rairden, R., Shine, R.A., Tarbell, T.D., Title, A.M., Wolfson, C.J., Elmore, D.F., Norton, A.A., Tomczyk, S.: 2012, *Solar Phys.*, **275**, 229. ADS: 2012SoPh..275..229S, DOI: 10.1007/s11207-011-9842-2.
Schrijver, C.J., De Rosa, M.L., Metcalf, T.R., Liu, Y., McTiernan, J., Régnier, S., Valori, G., Wheatland, M.S., Wiegelmann, T.: 2006, *Solar Phys.* **235**. 161. ADS: 2006SoPh..235..161S, DOI: 10.1007/s11207-006-0068-7.
Schröter, E.H.: 1962, *Z. Astrophys.* **56**, 183.
Schmieder, B., Hagyard, M.J., Ai, G., Zhang, H., Kalman, B., Gyori, L., Rompolt, B., Demoulin, P., Machado, M.E.: 1994, *Solar Phys.*, **150**, 199. ADS: 1994SoPh..150..199S, DOI: 10.1007/BF00712886.
Sun, X., Hoeksema, J.T., Liu, Y., Wiegelmann, T., Hayashi, K., Chen, Q., Thalmann, J.: 2012, *Astrophys. J.*, **748**, 77.
Švanda, M., Zhao, J., Kosovichev, A.G.: 2007, *Solar Phys.* **241**, 27 ADS: 2007SoPh..241...27, DOI: 10.1007/s11207-007-0333-4.
Welsch, B.T., Fisher, G.H., Abbett, W.P., Regnier, S.: 2004, *Astrophys. J.* **610**, 1148
Wang, H., Zirin, H.: 1992, *Solar Phys.* **140**, 41. ADS: 1992SoPh..140...41W, DOI: 10.1007/BF00148428.
Zhang, J., Li, L., Song, Q.: 2007, *Astrophys. J. Lett.* **662**, L35
Zhao, J., Couvidat, S., Bogart, R.S., Parchevsky, K.V., Birch, A.C., Duvall, T.L., Jr, Beck, J.G., Kosovichev, A.G., Scherrer, P.H.: 2012, *Solar Phys.* **275**, 375.
Zhao, J., Kosovichev, A.G., Sekii, T.: 2010, *Astrophys. J.* **708**, 304. ADS: 2012SoPh..275..375Z, DOI: 10.1007/s11207-011-9757-y.